Chapter 3

Localized Nano-Environment for Integration and Optimum Functionalization of Chlorophyll-*a* Molecules

P. Vengadesh

Additional information is available at the end of the chapter

http://dx.doi.org/10.5772/48707

1. Introduction

In recent years, there has been a growing trend of applying thin films containing natural pigments and dyes to various devices [1, 2] such as photovoltaic cells, optical waveguides and ultrafast optical switches in basic research, aiming at high performance and quantum efficiency. Though still at an experimental stage, much interest has been directed towards incorporating such photoactive materials into functionalized synthetic mediums or "artificial membranes" (AM). The photosynthetic biomaterials (PBMs) of interest such as the abundant Chlorophyll (Chl), in its native environment are contained within thylakoid membranes meant to provide a suitable host medium for optimum photoactivity to take place. Through millions of years of evolution, these membranes are constantly "rebuilt" and optimized to allow localized nano-environments for the integration of the synthesized PBMs. These nano-environments effectively introduce a higher area of light and nutrient absorption for Chl functionality. Inability to artificially replicate such localized nano-environment within the AM for nano-encapsulation of Chl molecules may be the key element hindering further progress in research into reconstituted PBMs for development of photovoltaic based devices and sensors.

Generally, suitable AM for impregnation of PBMs intended for photovoltaic studies require high levels of visible light transparency and penetration for photoreaction to occur efficiently and effectively. It is also of concern of making sure that the AM is totally inert to the active material used besides providing physical integrity, cellular-like viscosity, elasticity and humidity. A very important feature, internal humidity is required for optimum operation of most PBMs. For such a reason, AMs are required to have the ability to lock-in humidity and maintain a "gel-like" property similar to the natural lipid based membrane. By creating an almost natural-like environment, photosensitive biomaterials

such as the Chl molecules were shown to be able to retain their intrinsic properties for extended periods of time [3]. This is especially important due to the fact that Chl molecules are composed of extremely unstable compounds and therefore are readily destroyed by continuous exposure to light, oxygen, heat and acidic and alkaline substances. While most of the works [4] carried-out are concentrated into replicating photoswitching effects as in natural environment, not much effort was given into providing an in-depth comparative discussion into the effects of encapsulation of Chl within the AM matrix and photoresponse. The crucial the requirement is to create a compatible host medium for optimum photoreaction [3]. Such synthetic host environments are required to emulate the conventional tasks of natural lipid-based membranes. Generally, this involves electrons (and hydrogen ions) involved in the photosynthesis chain and nutrients that are transported based on two major stimulating responses, a trans-membrane concentration gradient [5] and upon light activation of photosensitive compounds [6].

In order to facilitate such complex processes, the material chosen for development of the synthetic host medium must recreate and maintain internal cellular viscosity. This would allow similar photo-induced steps to be maintained efficiently within the physical structure of the synthetic cell provided any loss of internal humidity is minimized or regulated by means of timed moisture absorption. In nature, the physical and viscous integrity of the plant cell is maintained by regulated fluid intake and elimination. Many different polymer materials offer the ability to be re-engineered to modify its' physical properties to mimic the native properties. One such polymer is carboxymethyl cellulose (CMC), which can be prepared in the form of an aqueous "gel-like" viscous solution with characteristics similar to a biological cell. CMC has been used in various practical fields [7, 8, 9]. In one such application [10], He Huang *et al.* studied electrochemical properties of proteins or enzymes such as Heme protein at CMC modified electrodes. They reported that CMC is able to provide a new and different matrix for immobilization of proteins.

2. Carboxymethyl cellulose as artificial membrane

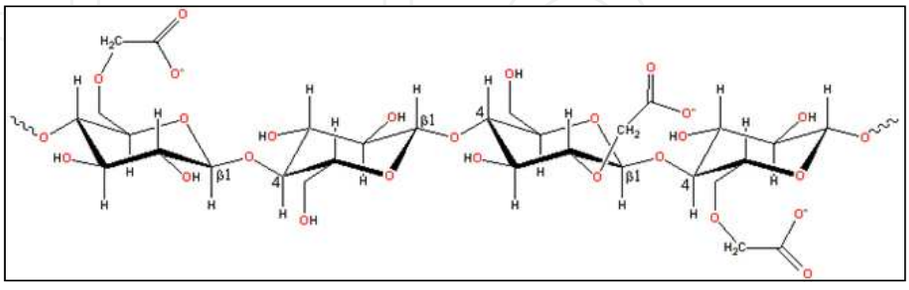

Figure 1. Structural unit of CMC [12].

Cellulose, the structural material of plant cell walls [11] is composed of repeating D-glucose units linked through ß-1, 4 glycosidic bonds (as shown in Figure 1). Under normal conditions, a tight packing of polymer chains is shown resulting in a highly crystalline structure. Such crystalline structures are able to resist salvation in aqueous media as a result

of existence of hydroxymethyl groups of anhydroglucose residues found above and below the plane of the polymer backbone. In order to increase water solubility, cellulose is treated with alkali resulting in swelling of the structure. This intermediate structure would then be reacted with chloroacetic acid, methyl chloride or propylene oxide to produce CMC, methyl cellulose (MC), hydroxypropyl cellulose (HPMC) or hydroxypropyl cellulose (HPC).

Recently, CMC have been extensively investigated for its potential as an AM material due to its desirable properties such as nontoxicity, biocompatibility, high hydrophilicity and excellent film forming abilities besides being not too expensive for large-scale commercial usage [13, 14]. Other positive factors are that these materials are non-ionic and compatible with surfactants, other water-soluble polysaccharides and salt [11]. CMC and its derivatives can also be dissolved in aqueous or aqueous-ethanol solutions for specific requirements. The resulting materials produced are generally odorless and tasteless, flexible and are of moderate strength, moderate to moisture and oxygen transmission, resistant to fats and oils [15-17]. CMC exhibits good film forming and suitable host medium properties. It is an excellent gas barrier material while at the same time allows water vapor diffusion. Many CMC based derivates have water vapor permeability comparable to Low Density Polyethylene (LDPE). Thus, their permeability or mechanical properties can be fine-tuned as dictated by the need of a specific application.

Proper understanding of various photochemical and photophysical properties of photosynthetic pigments in organic polymer matrix as an "in-vitro" biomimetic immobilizing media or AM, such as CMC may enable development of prototypes of PBM based devices. Advantages are attributed to more rigid stability and ability to control dispersion of incorporated photosynthetic molecules. CMC also acts as an effective dispersion agent for the active material and had been extensively studied and reviewed [18-23]. Formed as a film on top of the photosynthetic pigments, CMC are also observed to preserve photosensitivity for extended periods of time [3] while allowing crucial transfer of oxygen and moisture. Its potential functions and applications to film formation, coating and as AM can be achieved upon further extensive research on the methods of film and matrix formation and improvement of its internal properties. This would be crucial to warrant the increased need of considerations in potential functions and applications of CMC, especially involving Chl-*a* molecules when incorporated into the CMC matrix.

3. Photosynthetic biomaterial: Chlorophyll-*a*

Photosynthetic chloroplasts containing Chl molecules are found in green tissues of higher plants. They are mostly found in the form of Chl-*a* ($C_{55}H_{72}MgN_4O_5$) and Chl-*b* ($C_{55}H_{70}MgN_4O_6$), while other forms in nature are to be found as Chl-*c* ($C_{35}H_{30}MgN_4O_5$) and Chl-*d* ($C_{54}H_{70}MgN_4O_6$). These structures (Figure 2) differ only in the substituent at C-7, which is $-CH_3$ in Chl-*a* but –CHO in Chl-*b*. For Chl-*d* meanwhile, it is propionic acid substituent at C-17, which is isoprenoid alcohol phytol achieved by means of the esterification process.

Improvements over solid-state diagnostic methods in recent history enabled photosynthesis to be extensively studied in significant detail. Of particular interest are the photochemical and photophysical properties of photosynthetic pigments. Photosynthetic systems containing Chl-*a* molecules are popularly used for development of novel designs implementing the light-mediated processes rather than just for solar energy conversion [25]. Chl-*a* is considered significant for pigment studies in connection with the primary photosynthetic process, as well as light energy conversion. Chl exhibits a functional duality as energy collector and primary electron carrier since it plays an important role in the photosynthesis process occurring in plants and in some bacteria. Therefore, the absorption spectra of green plants have shown multiple forms of Chl. The molecules are arranged in a highly ordered state on grana thylakoid membranes and their local concentration of porphyrin rings is relatively high.

	Chlorophyll *a*	Chlorophyll *b*	Chlorophyll *c1*	Chlorophyll *c2*	Chlorophyll *d*
Molecular formula	$C_{55}H_{72}O_5N_4Mg$	$C_{55}H_{70}O_6N_4Mg$	$C_{35}H_{30}O_5N_4Mg$	$C_{35}H_{28}O_5N_4Mg$	$C_{54}H_{70}O_6N_4Mg$
C3 group	$-CH=CH_2$	$-CH=CH_2$	$-CH=CH_2$	$-CH=CH_2$	-CHO
C7 group	$-CH_3$	-CHO	$-CH_3$	$-CH_3$	$-CH_3$
C8 group	$-CH_2CH_3$	$-CH_2CH_3$	$-CH_2CH_3$	$-CH=CH_2$	$-CH_2CH_3$
C17 group	$-CH_2CH_2COO-$Phytyl	$-CH_2CH_2COO-$Phytyl	-CH=CHCOOH	-CH=CHCOOH	$-CH_2CH_2COO-$Phytyl
C17-C18 bond	Single	Single	Double	Double	Single
Occurrence	Universal	Mostly plants	Various algae	Various algae	cyanobacteria

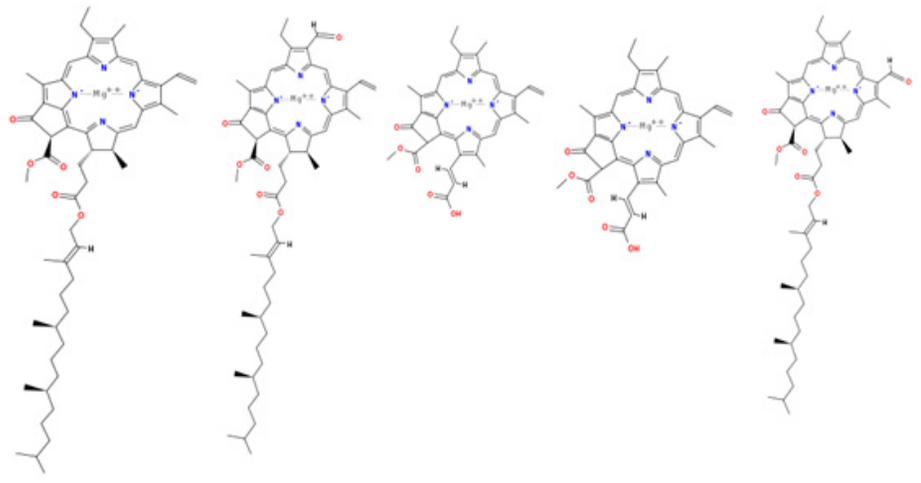

Figure 2. Structure of chlorophylls [24].

Photosynthetic organisms are able to oxidize water, upon absorption of sunlight, to produce oxygen. In higher plants this process takes place in the thylakoid membranes located inside the chloroplast. These membranes have two key reaction centers, P700 and P680, both of which operate in two distinct photosystems, photosystem I (PSI) and II (PSII) and consist of Chl-*a* molecules. The oligomeric nature of P680 "*in-vivo*" is a matter of considerable interest. Some studies suggest that P680 composed of one molecule of Chl-*a* [26-28], while others proposed it as a dimer [29-31]. Absorption and fluorescence spectra of dry Langmuir-Blodgett multilayers

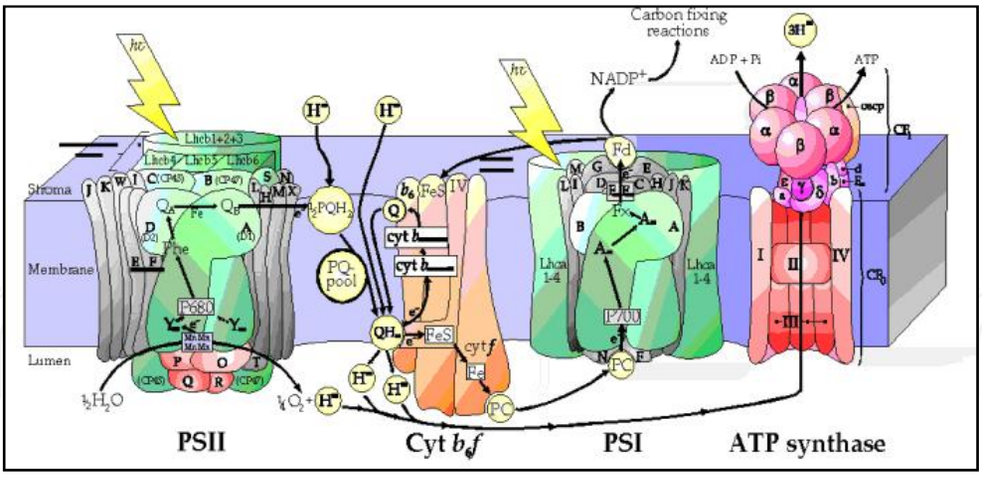

Figure 3. Simple illustration showing the PSI and PSII processes involved in photosynthesis [32].

of Chl-*a* present similarities with those observed for the P680 or P700 and its electron acceptors make up PSI, whereas P680 and its electron carriers make up PSII as shown in Figure 3. The latter is the site where the primary reaction takes place. Both Chl-*a* and Pheophytin-*a* (Phe-*a*) are pigments known to be present in this reaction center where they act as the primary electron donor (P680) and acceptor respectively. Also present in the PSII reaction center are the plastoquinones, quinones A (QA) and B (QB) that always act in series with the carotenoid molecules. Pigments that undergo electron transfer reaction are bound to the Dl-Dz-Cytb559 protein complex, an integral part of the PSII core complex. The reaction center of PSII probably contains four molecules of Chl-*a*, two molecules of Phe-*a* and two quinones. Compared to the PSII reaction center, the PSI reaction center is more complicated. Its Chl-*a* content varies between 100 and 200 molecules, most of which are not photochemically active, but serve as part of the antenna system that absorbs light and transfers energy to the reaction centers. Excitation of PSII drives the transfer of an electron from P680 to a Phe-*a* molecule, which immediately reduces QA.

After being transferred to QB, the electron flows to the oxidized Chl-*a* in PSI (P700 through electron transport chain) provoking splitting of H_2O to O_2 through four Manganese (Mn) atoms, which are probably bound to the proteins that hold P680. This splitting is followed by release of an electron used to reduce P680 to its original state. Same process happens in PS1 and the Chl-a in the PSI is reduced to its original states by electron from PSII. The excited electron in PSI is sent through the electron transport chain and the electron will be used to produce NADPH. During the process, electron traveling down the electron transport chain produces a chemio-static potential, which will be used by ATP synthesizer to synthesis ATP from ADP. The resulting ATP and NADPH will then be used to produce sugar from CO_2.

4. Impregnation of Chlorophyll-*a* within carboxymethyl cellulose

There are various methods to prepare "*in-vitro*" biomimetic photosynthetic films, such as spin-coating, Langmuir-Blodgett, sol-gel and electrodeposition methods. However, only

spin-coating method enables true impregnation of Chl-*a* molecules due to the nature of the process to yield entrapped chromophores within the CMC matrix. When mixed with the right concentration of CMC and spin-coated onto solid substrates, a high dispersion of Chl-*a* molecules was observed. This is because cellulose derivatives are excellent dispersion agents widely used in the detergent, food, paper, textile, pharmaceutical and paint industries.

An important feature of a good dispersive agent is to provide a suitable matrix environment to the active material. For a complex photosynthetic biomolecule such as Chl-*a*, this becomes extremely crucial for optimum photoactivity to be achieved. Chl-*a* molecules embedded within the CMC and other cellulose derived polymer matrix films were able to exhibit potential in mimicking the property as photosynthetic pigment "*in-vivo*" systems. In one such work, Wrobel et al. [23] reported Chl-*a* molecules in polymer matrix of polyvinyl alcohol (PVA) and cellulose derivatives. In their work, Chl-*a* in monomeric form, dimer and nitrocellulose complex (NC) forms were investigated. The concentration of PVA used was 1 g per 9 ml dimethyl sulfoxide (DMSO) whereas concentration of NC was either 0.4 g per 5 ml DMSO (low-NC sample) or 2 g per 5 ml DMSO for high-NC sample. This results in final concentrations of Chl-*a* in films at ($1x10^{-7}$) and ($5x10^{-1}$) mol/g. Results indicated similarity of optical properties for monomeric Chl-*a* in PVA and NC by obtaining a strong α-band with a maximum at 670 nm while a small component was observed at about 720-730 nm. Results associated with optical properties confirmed that the optical spectrum was dependent on concentrations of the polymer matrix. At the higher concentration, contribution of a significant fraction of dimers shouldering around 740 nm seems to be higher compared to the absorption peak at 670 nm, indicating formation of a dimeric form of Chl-*a* molecule. A small hump at 680 nm, characteristic feature of Chl-NC complex was obtained in high-NC. Again this indicated a very slight contribution of the monomeric form as presented by the emission spectrum.

The present work looks into the possibility of employing CMC as the AM material and investigates its localized nano-environment for the impregnation of Ch-*a* pigments and optimum photosensitivity. Following sections will provide information on materials preparation followed by experimental results and in-depth discussions. The last section meanwhile would state major conclusions and findings of the research.

5. Optimum CMC concentration effect

For the current work, a target Chl-*a* suspension in chloroform ($CHCl_3$) was prepared as suggested in literature [22, 23]. A concentration of 0.45 mg/ml was prepared and stored in a fridge for three days prior to usage. Seven concentrations of CMC gel-like aqueous solution (6, 12, 18, 24, 30, 36 and 41 mg/ml) were prepared for the purpose of investigating productive photoactivity based upon optimum concentration of AM concentration. From the method employed in literature [33], CMC was dissolved in deionised (DI) water and ethanol according to its solvent ratio in miligrams as shown in Table 1. The CMC solutions

were then ultrasonificated for an hour and magnetic stirred at 70°C overnight. Solutions obtained appeared transparent and did not precipitate from the solvent.

Solvent ratio (DI:Ethanol:CMC), *mg*	Mass of CMC, *mg* (±0.1)	Volume of DI, *ml* (±0.1)	Volume of Ethanol, *ml* (±0.1)	Concentration, *mg/ml*
120:38:1	50	6.0	2.41	6
60:19:1	100	6.0	2.41	12
42:12:1	50	2.1	0.76	18
30:9.5:1	200	6.0	2.41	24
25:7:1	85	2.1	0.76	30
20:6:1	300	6.0	2.41	36
18:5:1	100	1.8	0.63	41

Table 1. Preparation of different concentrations of CMC suspension.

In order to investigate possible enhanced properties of CMC-Chl-*a* films prepared at different spin rates, its corresponding optical spectra were obtained. As seen from the graphs in Figure 4, similarity of absorption peaks of Soret and α-bands at 434 and 675 nm respectively were observed. It confirms retention of the native spectroscopic properties of Chl-*a* preserved within the CMC matrix. In certain CMC concentrations (Figure 4(d) and (g)), higher absorptions were registered at both bands compared to free Chl-*a* molecules suggesting applications in "in-vitro" biomimetic immobilizing media in synthetic mixture [34]. Elsewhere [22, 23], higher values of absorbance peaks have been reported.

However in the present work, intense absorption at α-band were obtained when Chl-*a* molecules were impregnated into the CMC matrix with concentration of 24 mg/ml and especially at 1000 rpm (Figure 5). At this concentration and rpm, the optimum dispersive concentration for Chl-*a* molecules possibly allows enhanced photoreaction to occur when evenly distributed in polymer hydrogel forms. Higher photosensitivity was also observed for the other films when prepared at the optimum spin rate. Careful observation of the graphs in Figure 5 also demonstrated a sharp and narrow absorption peak at 415 nm of 10 nm width attributed to the Soret band instead of the usual 435 nm in free Chl-*a* molecules. Upon increase in matrix concentration, the characteristic peak observed was observed to generally shift to a higher angle. The resulting blue shift may be due to even existence of Chl-*a* molecules rather than being aggregated within the CMC support. This explains the higher depth values obtained at CMC concentrations of 18 and 30 mg/ml as compared to other concentrations. Since absorption intensity is also dependent on film thickness, the resulting decrease in absorption peaks of CMC-Chl-*a* films of increasing spin rates is quite understandable. Rougher surfaces register lower photosensitivity even at the optimum CMC concentration. This may be due to spin rate influencing colloid present within the film environment besides the concentration factor.

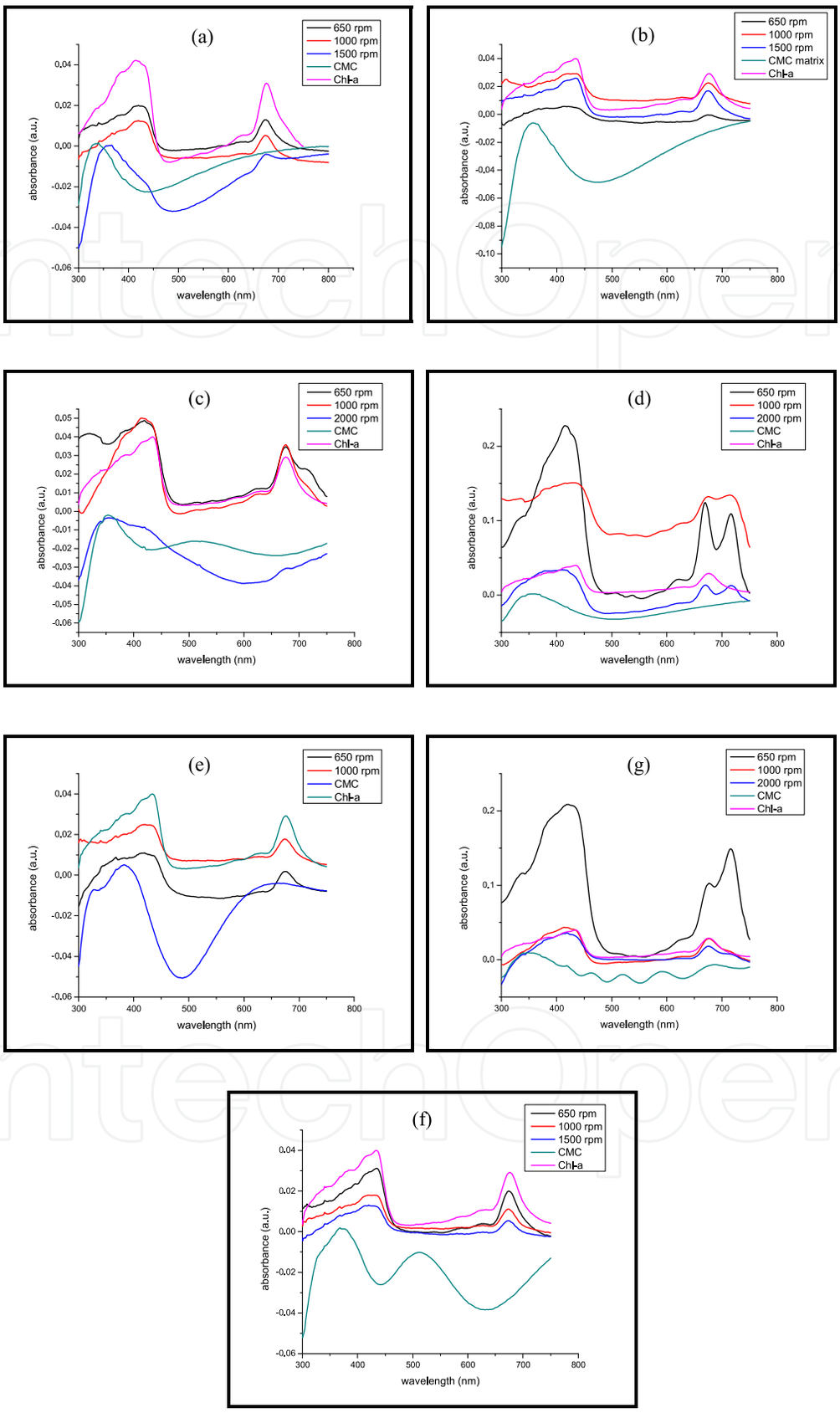

Figure 4. CMC-Chl-*a* thin films at concentrations of (a) 6, (b) 12, (c) 18, (d) 24, (e) 30 and (f) 41 mg/ml of CMC matrix respectively.

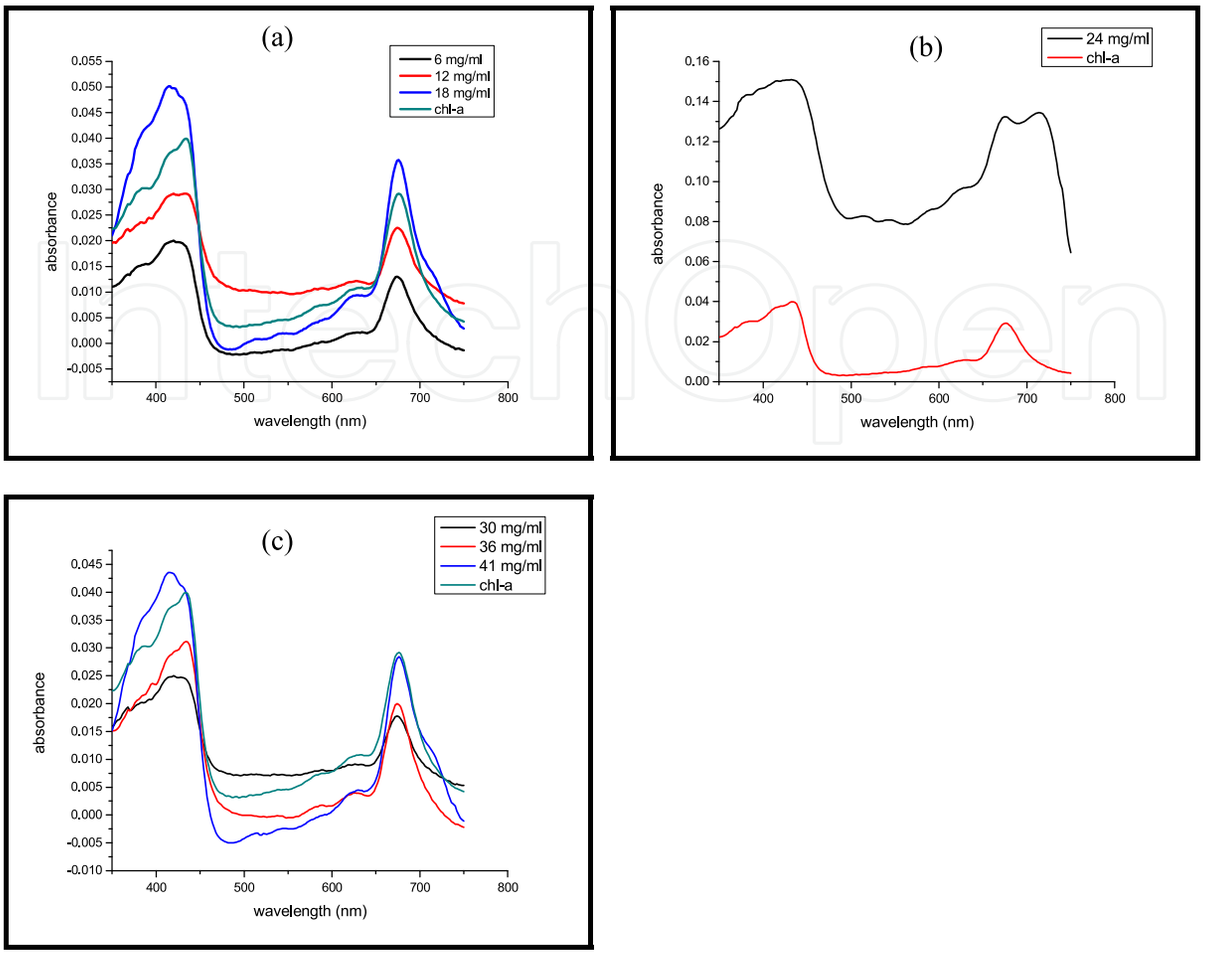

Figure 5. (a) Absorption spectra of Chl-*a* in CMC matrix films and Chl-*a* (5 x 10^{-4} M) in chloroform for CMC matrix concentration below 24 mg/ml. (b) A similar spectrum has been obtained for Chl-*a* (at the same pigment concentration) in CMC matrix of concentration 24 mg/ml showing a much higher peak (roughly 3 times) and in (c) CMC matrix of concentration greater than 24 mg/ml.

The optimum CMC concentration at 24 mg/ml with the most intense absorption at α-band registered the largest full width half maximum contributed by a significant fraction of dimers shouldering around 720 nm. High solvent content also provides an aqueous media for photoreaction of Chl-*a* molecules resulting in a loose CMC structure. This in turn provides a suitable nano-environment for the impregnation of the photosynthetic pigments. Such an environment allows uniform distribution and dispersion of the molecules within the synthetic medium for enhanced photosensitivity. Higher solvent volume reflects higher concentration of CMC aqueous media, in agreement with literature [23] stating influence in the absorption spectra of Chl-*a* films. Therefore, the native state of Chl-*a* molecules were still retained in cellulose derivatives even in high concentrations of CMC. The work also suggests self-association of Chl-*a* molecules by means of a hydrogen-bonding nucleophile, such as water or solvent. Higher absorption peak intensity values were obtained at the optimum concentrations; comparable to previous works elsewhere [22]. The graphs in Figure 6 show optical absorbance of CMC-Chl-*a* films over time for CMC matrix concentrations of 18, 24 and 41 mg/ml, respectively. In this experiment, spectroscopic

characterization was carried-out every week for a month for the films with higher α-band peaks compared to free Chl-*a* molecules in chloroform.. Studying absorbance peaks at the α-band indicates photophysical functionality of Chl-*a* molecules to synthetic mixtures. Encapsulating the pigments with the CMC layer slows down oxygen reduction process from oxidizing the Chl-*a* molecule in the films prepared. As a result, retention of the photosynthetic nature of the reconstituted Chl-*a* molecules are maintained successfully.

In a previous work [35], researchers have reported loss of spectroscopic properties when Chl-*a* molecules deposited as thin films were exposed directly to oxygen. As such, we have shown that by impregnating Chl-*a* molecules into CMC matrix forming thin films, an encapsulating effect is achieved which prolongs the optical functionality of the photosynthetic pigment. Eventual decay in photosensitivity may be attributed to the fact that some molecules at air-solid interface may not be totally encapsulated against the elements due to the nature of the process. In addition, CMC-Chl-*a* films also exhibit a small blue shift of the optical absorbance from 674 to 672 nm, indicative of gradual structural changes in the Chl-*a* molecules. At CMC concentrations of 18, 24 and 41 mg/ml, the films are more likely to have loose matrix structure in its hydrogel form. This results in localized nano-environment for suitable entrapment of Chl-*a* molecules for optimum photoactivity indicated by high value of absorption peak intensity at the α–band.

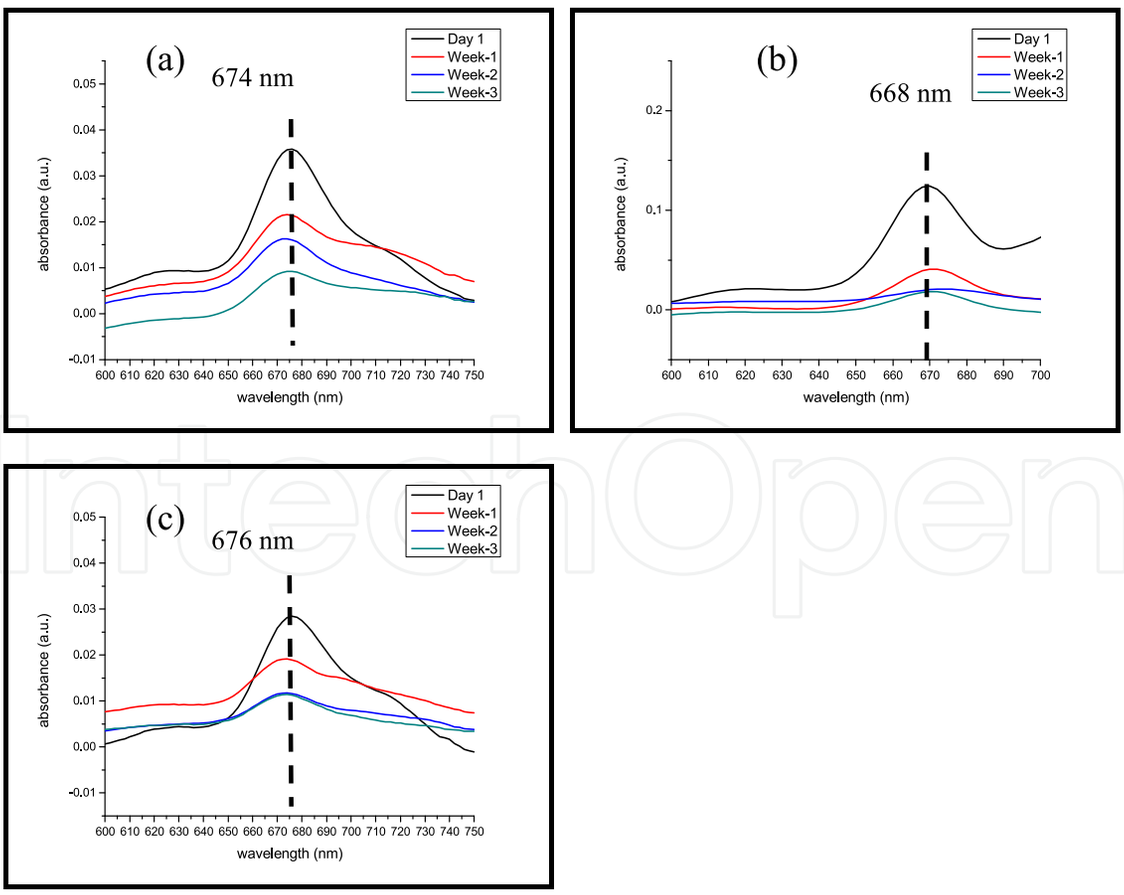

Figure 6. Absorption spectra at α-band for CMC concentrations of (a) 18, (b) 24 and (c) 41 mg/ml respectively.

6. Structural properties of CMC-Chl-*a* films

Figure 7 shows XRD measurement of the CMC-Chl-*a* films prepared at spin rate of 1000 rpm and different concentrations. Regardless of the spin rate effects, similarity of XRD patterns for all matrix concentrations in the range of 2θ between 10° to 80°, confirms existence of Magnesium nitrate di(N-N-dimethylurea) tetrahydrate and Magnesium nitrate-6-ethanol identified as crystalline phase.

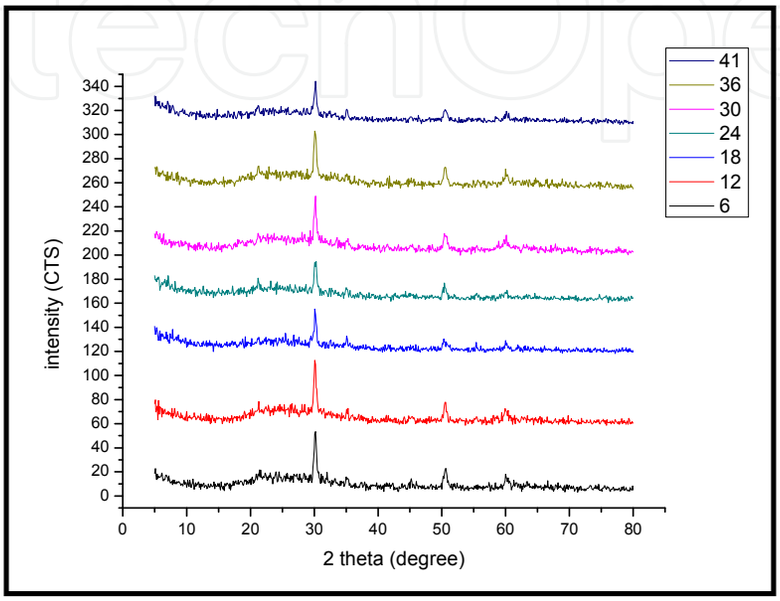

Figure 7. XRD patterns of CMC-Chl-*a* films prepared at 1000 rpm and different CMC concentrations.

In Figure 8, the most intense peak at 2θ occurs at 30.1° referring to the Chl-*a* characteristic peak which was shifted to higher angle when films were prepared in higher concentrations. Broadening of diffraction lines was also observed when films were prepared in the optimum CMC concentration of 24 mg/ml resulting in expansion of pores in the films [36]. This also indicates the existence of a smaller unit cell being the dominant effect causing the breadth of the diffraction lines [37]. Based on XRD results showing several sharp peaks, the polycrystalline nature of Chl-*a* molecules impregnated within the organic polymer matrix could be confirmed. Using Scherer equation, the grain size of a single Chl-*a* molecule is calculated to be about 10 nm of length confirming existence of nanocrystalline structures of the photosynthetic pigments.

Figure 9 represents the FESEM-EDX imaging measurement, which is in good agreement with the XRD measurement. Existence of elements such as magnesium oxide, sodium, oxygen and indium arsenide elements are traced within the prepared colloids. Since CMC may interact with Chl-*a* molecules and influence morphology of the films formed on ITO substrates, AFM investigation was performed to obtain morphological information of Chl-*a* embedded into the CMC polymer matrix. Figure 10 is AFM images showing morphology of CMC-Chl-*a* colloids at CMC matrix concentration of 24 mg/ml deposited on ITO slides at the spin rate of 1000 rpm. Generally, the colloids were in long and unfolded successions of aggregates, regardless the concentrations of the matrices possibly due to different colloidal interaction with the substrate.

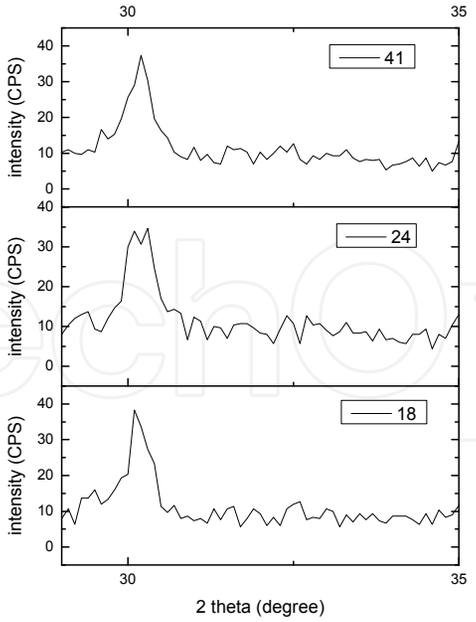

Figure 8. XRD patterns of the films in the region of 2θ = 29° - 35° for Chl-*a* embedded in different concentrations of CMC matrix: (a) 18, (b) 24 and (c) 41 mg/ml.

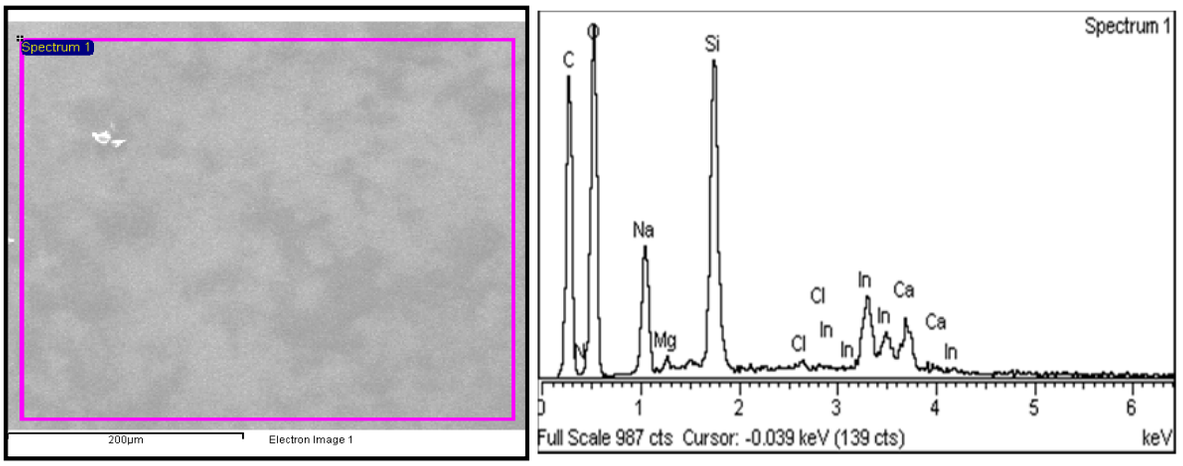

Figure 9. FESEM-EDX analysis of CMC-Chl-*a* thin film prepared using 24 mg/ml of CMC aqueous solution. EDX images were obtained under 300X magnification with accelerating voltage of 20 kV within a processing time of 5 seconds.

According to Boussaad *et al.* [36], CMC-Chl-*a* complex in solution with polar solvents usually carries a net positive charge. As a consequence, complex-substrate interaction would be influenced by repulsive or attractive interaction as a result of the presence of this charge. The repulsive interaction induced by the ITO surface may cause the colloids of the complex to unfold into long successions of aggregates. It was also clear from literature that long and unfolded successions of aggregates were observed when the complex is deposited onto hydrophilic surfaces, such as gold [38]. Results show that different concentrations of CMC aqueous solutions used to prepare thin films at certain spin rates could produce different degrees of orderly distribution of CMC-Chl-*a* complex across the substrate. Resulting thin films as shown in Figure 11 therefore show differing surface roughness. In these films,

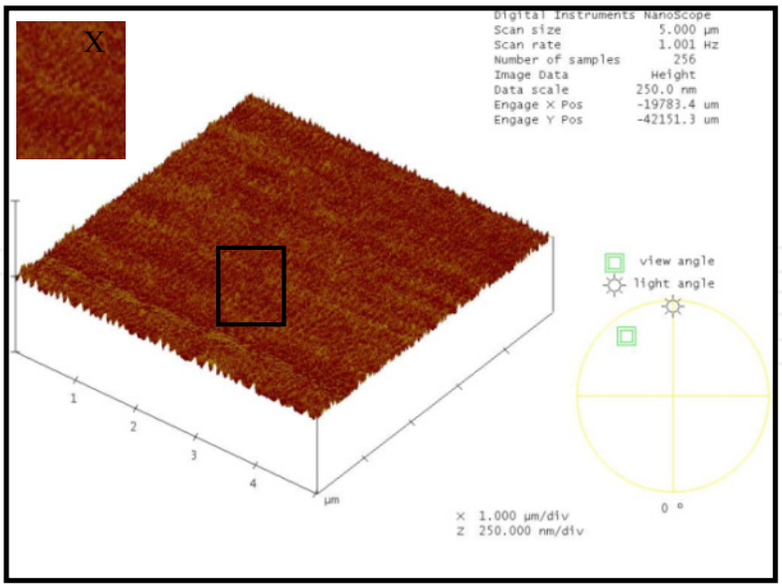

Figure 10. AFM images of CMC-Chl-*a* films deposited onto ITO slides with CMC concentration of 24 mg/ml. Micrograph X was cropped and enlarged from the square box in the AFM image.

crescent shaped Chl-*a* colloids of length of 10 nm are observed throughout the substrate. Such uniformity of molecular structures was observed to decrease at high concentrations, an observation in good agreement with the XRD results. This may also explain the formation of dimer association in the aggregates. Arrangement of dimers within the nanocrystal reflects the crystalline structure of the microcrystalline Chl-*a*. The differences between dimer and microcrystal structures of Chl-*a* in the films depend strongly on the dissociation and association of the dimers. Usually, excess of solvent used in the CMC matrix compete with the nanocrystal bonding and causes the aggregates to dissociate resulting in rougher surfaces. However, angular velocity of the spinning method may also influence the formation of dimer association in the aggregation [21].

Figure 12 summarize the roughness (a) and depth analysis (b) respectively for CMC-Chl-*a* films at different spin rates. In general, from Figure 12(a), it could be deduced that Chl-*a* molecules were well dispersed in the CMC matrix. This results in surface mean roughness in the range of 4 to 19 nm, quite comparable to other deposition techniques [22, 23]. The values of roughness were found to decrease as the CMC concentrations increases. Roughness meanwhile increases after achieving the optimum concentrations for each spin rates. Optimum concentration of CMC was achieved at 36 mg/ml for the spin rate of 650 rpm which results in mean roughness of about 3.86 nm. At spin rates of 1000 and 1500 rpm, optimum concentration was achieved at 18 and 30 mg/ml respectively. Hence, it could be assumed that mean roughness values of the CMC-Chl-*a* films were independent to spin rate. Higher spin rates did not produce a smoother film except for the 30 mg/ml concentration of CMC. The values actually decreased when films are spun at higher spin rates.

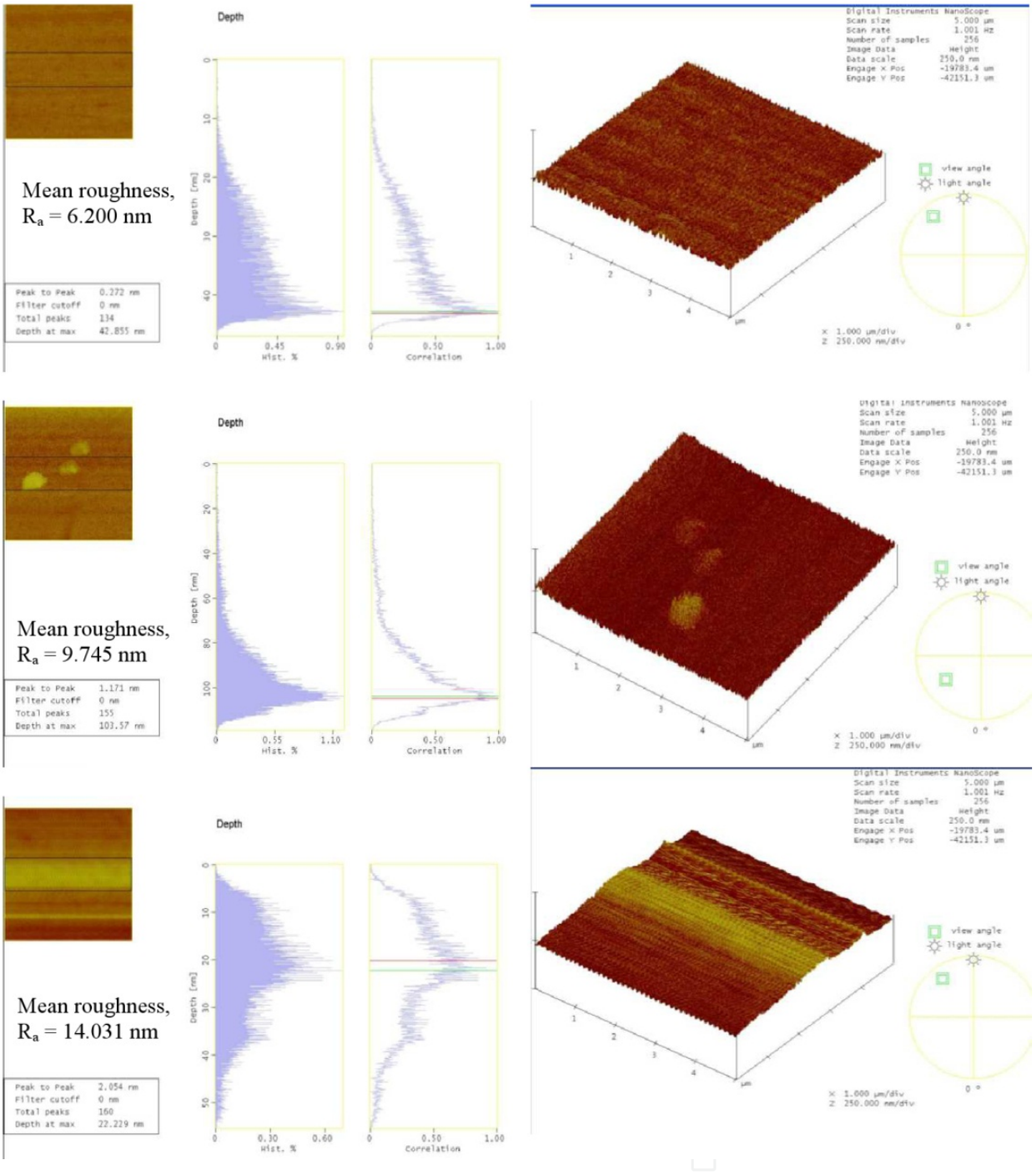

Figure 11. AFM images of CMC-Chl-*a* thin films prepared at spin rates of 650, 1000 and 1500 rpm at CMC concentration of 24 mg/ml.

Results of depth analysis for CMC-Chl-*a* films indicate that the prepared concentrations of CMC aqueous solution were able to produce better distribution of Chl-*a* molecules across the substrate. As shown in Figure 12(b), this results in maximum depth in the range between 17 to 100 nm. As observed from the roughness analysis results, depth results also confirm that the films prepared at the spin rate of 1000 rpm shows the smallest deviation between the values. The values increased with spin rates resulting in thicker films due to dissociation

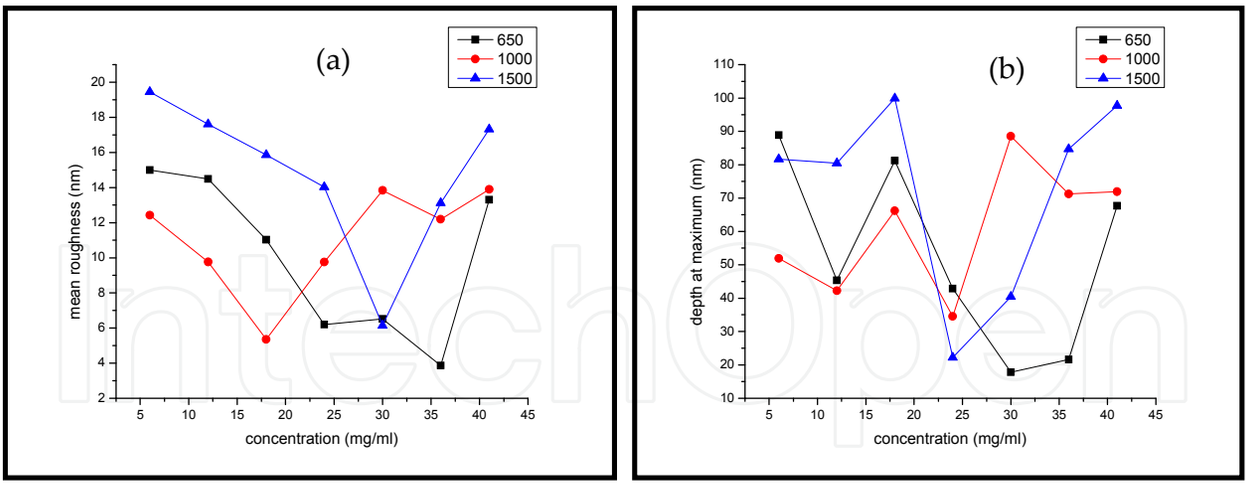

Figure 12. (a) Mean roughness and (b) depth analysis of CMC-Chl-*a* films.

of Chl-*a* aggregates within CMC matrix. Therefore, weak affinity between Chl-*a* colloids and the ITO substrate could be deduced, as reported in literature [13]. When weakly binding onto ITO surfaces, solvent bound molecules were found harder to be controlled by spin rate and thus create thicker films. However, for CMC-Chl-*a* films prepared in optimum matrix concentration of 24 mg/ml, the values were observed to decrease with increase in spin rates.

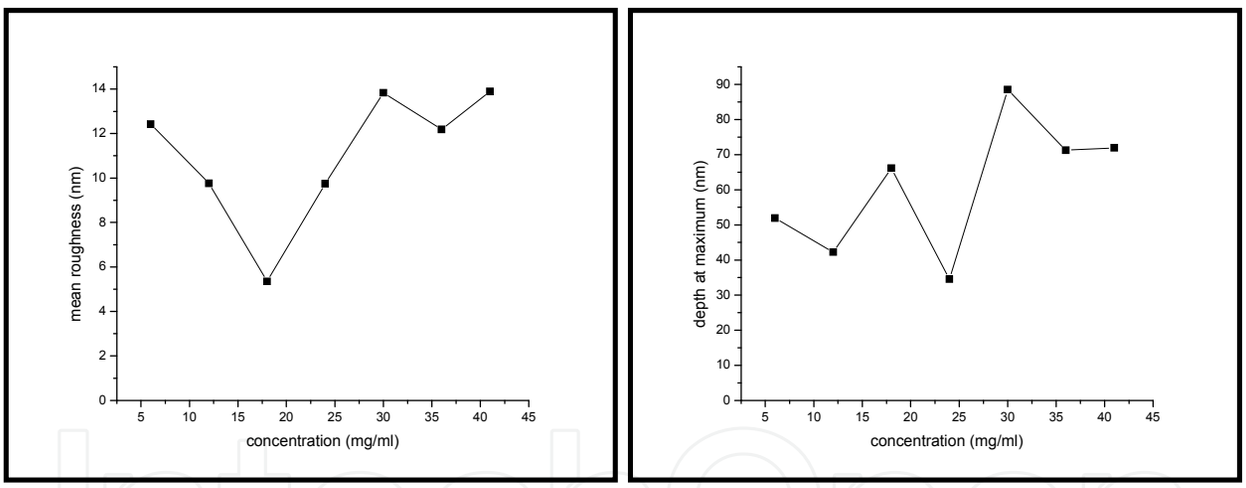

Figure 13. (a) Mean roughness and (b) depth analysis of CMC-Chl-*a* films at spin rate of 1000 rpm.

In summary, the Chl-*a* molecules were well dispersed within the cellulose derivative while achieving desirable thickness and smooth thin films regardless of spin rate. AFM images also confirmed that the spin coating technique could be employed to synthesize nanocrystalline molecular structures of Chl-*a* molecules at different concentrations of CMC matrices. Particularly, CMC concentration of 24 mg/ml exhibits the optimum AM concentrations at the spin rate of 1000 rpm as shown in Figure 13(a). Depth analysis meanwhile in Figure 13(b) concludes molecular structures smaller than 70 nm at concentrations below 24 mg/ml. These findings indicate strong affinity between high concentrations of CMC and ITO substrate. Upon strongly binding to ITO surface, solvent bound molecules were found easier to be controlled by the spin rate and thus create a new surface for the CMC-Chl-*a* film. This new surface might bring about the formation of

smoother and thinner film morphology. However, excess solvent used competes with nanocrystal bondings causing the aggregates to dissociate resulting in rougher surfaces.

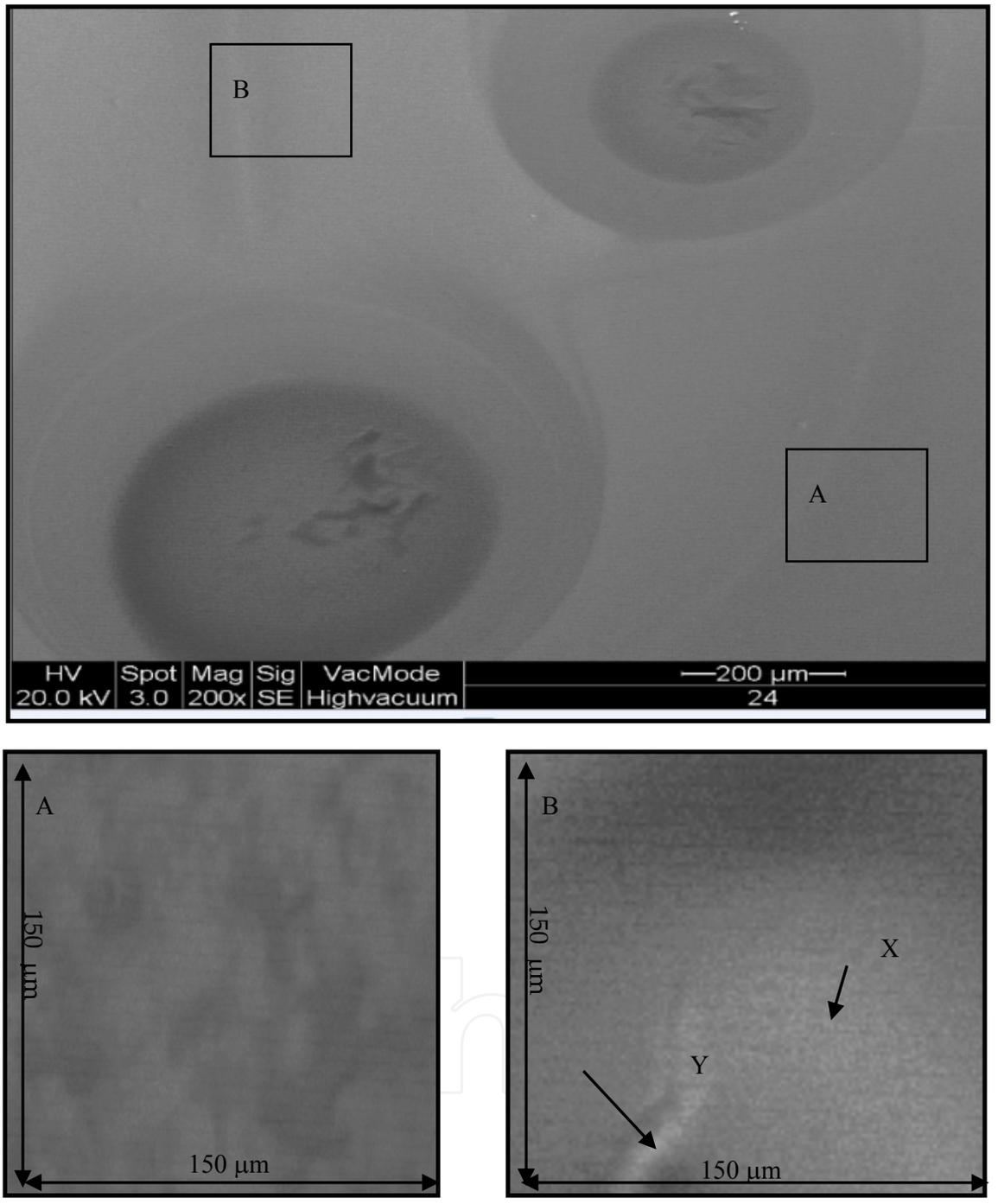

Figure 14. FESEM views of spin-coated ITO for CMC-Chl-*a* films. Micrograph A and B were cropped and enlarged three times from the main micrograph

FESEM measurements were also performed to further confirm existence of nanocrystal form of Chl-*a* molecules in CMC matrices at the optimum concentration and spin rate. Figure 14 shows the micrographs obtained for CMC concentration of 24 mg/ml at 1000 rpm. In a separate work [11] involving dry CMC films on pyrolytic graphite electrodes, it was reported

that large amount of water absorbed forming hydrogel by obtaining a wide leaf-like structure without formation of crystals. However, the SEM top views of CMC-Chl-*a* films in the present study show a different surface morphology. The aggregates were compressed within the colloid resembling large cloud-like thin sheets and form a very dense complex on the ITO surface (micrograph A). Micrograph B meanwhile shows orderly distributed molecular structures highlighted by the spots within the square box B in the main micrograph of Figure 14. These spots were distributed randomly across the substrate indicative of the uniformity of the fabricated films, confirming arrangement of dimers within the nanocrystalline structures found in the colloids (X). Organization of Chl-*a* molecules reflects the optical properties of the nanocrystalline molecular structure. Some small "island-like" formation in highly packed groups (Y) found in the colloids (bright spots) is actually Chl-*a* dimers [23] embedded into the CMC matrix forming tight interactions. They are responsible for successful retention of Chl-*a* molecules within the films and provide a "membrane-like" environment for entrapment and enhanced functionality of the photosynthetic pigments.

7. General conclusions

This study suggests the self-association of Chl-*a* in cellulose derivative matrices utilizing the spin-coating technique while maintaining its native spectroscopic characteristics when reconstituted into CMC matrix. It highlights the potential of encapsulating Chl-*a* and other PBMs with the CMC acting as the AM. Successful prolonged retention of the Chl-*a* molecules' spectroscopic properties within the CMC-Chl-*a* films was also demonstrated. Considerably smooth film surfaces were obtained comparable to other conventional deposition techniques.

High absorption peak intensities of the Soret and α-bands indicate well-dispersed Chl-*a* molecules within the CMC phase. Lower solvent content or lower concentration effect causes the Chl-*a* aggregation to exhibit weak affinity to the ITO substrate. As a consequence, it becomes harder to control film morphology at high spin rates resulting in thicker films. Comparable results were also deduced from XRD patterns highlighting retention of the native state of Chl-*a* molecules for all CMC matrix concentrations.

Morphological characterization confirms the nanocrystal formation of Chl-*a* molecules in all CMC concentrations of the synthetic film. The colloids were observed to be in long and unfolded successions of aggregates indicating self-association of Chl-*a* molecules in the cellulose derivative matrix. Maximum depth was found to be in the order of 100 nm and would further decrease if the films were prepared in optimum CMC concentration of 24 mg/ml. This may well suggest dimer association in the aggregation by further observing the absorption band at 720 nm. The arrangement of dimers within the nanocrystal in turn reflects the crystalline structure of the overall microcrystalline Chl-*a* structure in the films prepared.

Author details

P. Vengadesh
University of Malaya, Malaysia

Acknowledgement

The experimental section was supported in parts by the Ministry of Higher Education, Fundamental Research Grant Scheme (FRGS) grant number FP011/2008C, University of Malaya Postgraduate Research Fund grant number IPPP/UPDit/Geran(PPP)/PS225/2009A and High Impact Research (HIR) grant number J-21002-7-3823. The author is also grateful to his postgraduate student, Wong Yee Wei who was reponsible for the data collection.

8. References

[1] Ioana L, Nicoleta B, Rodica N, Alina M, Florin M, Ion I, Aurelia M (2010) Encapsulation of Fluorescence Vegetable Extracts within a Template Sol-Gel Matrix. optical materials 32: 711-718.

[2] Zhaoqi F, Chuanhui C, Shukun Y, Kaiqi Y, Rensheng S, Daocheng X, Chunyu M, Xu W, Yuchun C, Guotong D (2009) Red and Near-Infrared Electroluminescence from Organic Light-Emitting Devices based on a Soluble Substituted Metal-Free Phthalocyanine. optical materials 31: 889-894.

[3] Wong YW, Vengadesh P (2011) Synthesis, Structural and Spectroscopic Properties of Encapsulated Chlorophyll-*a* Thin Film in Carboxymethyl Cellulose. j. of porpyrin and phythalocyanine 15: 122-130.

[4] Itamar W, Shai R (2003) Control of the Structure and Functions of Biomaterials by Light. ang. chemie int. ed. in eng. 35(4): 367-385.

[5] Mohamed El-Anwar HO, Fatma E (1988) Photosynthetic Electron Transport under Phosphorylating Conditions as Influenced by Different Concentrations of Various Salts. j. exp. bot. 39(7): 859-863.

[6] Devens G, Thomas M (2002) Active Transport of Ca^{2+} by an Artificial Photosynthetic Membrane. nature 420(6914): 398-401.

[7] Hemadeh O, Chilukuri S, Bonet V, Hussein S, Chaudry IH (1993) Prevention of Peritoneal Adhesions by Administration of Sodium Carboxymethyl Cellulose and Oral Vitamin E. surgery 114(5): 907-10.

[8] Lin D, Zhao Y (2007) Innovations in the Development and Application of Edible Coatings for Fresh and Minimally Processed Fruits and Vegetables. In: Comprehensive Reviews in Food Science and Food Safety. Oregon: Institute of Food Technologists.

[9] Minami N, Kim Y, Miyashita K, Kazaoui S, Nalini B (2006) Cellulose Derivatives as Excellent Dispersants for Single-Wall Carbon Nanotubes as Demonstrated by Absorption and Photoluminescence Spectroscopy. applied physics letters 88(9): 093123-093126.

[10] He Huang PH (2003) Electrochemical and Electrocatalytic Properties of Myoglobin and Hemoglobin Incorporated in Carboxymethyl Cellulose Films. bioelectrochemistry 61: 29-38.

[11] Nisperos-Carriedo MO (1994) Edible Films and Coatings based on Polysaccharides. In: Krochta JM, Baldwin EA, Nisperos-Carriedo MO, editors. Edible Coatings and Films to Improve Food Quality. Lancaster: Technomic Publishing Company Inc. pp. 305–35.

[12] Carboxymethyl Cellulose.Retrieved from: http://www.Isbu.ac.uk/water/hycmc.html
[13] Bourtoom T (2008) Edible Films and Coatings: Characteristics and Properties. journal of international food research. 15(3): 237-248.
[14] Savage AB, Young AE, Maasberg AT (1954) Cellulose and Cellulose Derivatives. In: Ott E, Sourlin HM, Grafflin MW, editors. High Polymers. New York: Interscience.
[15] Nelson KL, Fennema OR (1991 Methylcellulose Film to Prevent Lipid Migration in Confectionery Products. j. food sci. 56: 504–509.
[16] Gennadios A, Hanna MA, Kurth B (1997) Application of Edible Coatings on Meats, Poultry and Seafoods: A Review. lebens wissen technol. 30: 337–350.
[17] Kaistner U, Hoffmann H, Donges R, Hilbig J (1997) Structure and Solution Properties of Sodium Carboxymethyl Cellulose. colloids surf. A 123: 307–328.
[18] Jacobs EE, Vatter A E, Holt AS (1953) Crystalline chlorophyll and bacteriochlorophyll. journal of chemistry and physics 21: 2246-2279.
[19] Katz JJ (1994) Long wavelength chlorophyll. spectrum 7(1): 1, 3-9.
[20] Oureriagli A, Kass, H, Hotchandani S, Leblanc RM (1992) Analysis of Dark Current-Voltage Characteristics of Al/Chlorophyll a/Ag Sandwich Cells. journal of applied physics 71(11): 5523-5530.
[21] Kassi H, Hotchandani S, Leblanc RM (1993) Hole Transport in Microcrystalline Chlorophyll a. appl. phys. lett. 62(18): 2283-2285.
[22] Pasquale LD, Lucia C, Pinalysa C, Paola F and Angela A (2004) Photophysical and Electrochemical Properties of Chlorophyll a-Cyclodextrins Complexes. bioelectrochemistry 63: 117– 120.
[23] Wróbel D, Planner A. and Perska B. (1996) Time-Resolved Delayed Luminescence of Chlorophyll α in Anhydrous Polymer Systems. spectrochimica acta part a 52: 97-105.
[24] Chlorophyll-a. Retrieved from: http://en.wikipedia.org/wiki/Chlorophyll
[25] Mehraban Z, Farzaneh F, Shafiekhani A (2007) Synthesis and Characterization of a New Organic-Inorganic Hybrid NIO-Chlorophyll-*a* as Optical Materials. optical materials 29: 927-931.
[26] Photosystem II. Retrieved from: http://beckysroom.tripod.com/summary1.htm
[27] Rodrigo FA (1953) Preliminary Note on Experiments Concerning the State of Chlorophyll in the Plant. biochim. biophys. acta 10(2): 342.
[28] Jacobs EE, Holt AS, Rabinowitch E (1954) The Absorption Spectra of Monomolecular Layers of Chlorophyll *a* and Ethyl Chlorophyllide *a*. j. chem. phys. 22: 142-144.
[29] Ke B (1966) In: Vernon LP, Seely GR, editors. The Chlorophylls. New York: Academic Press Inc. pp. 253.
[30] Chapados C, Leblanc RM (1977) Aggregation of Chlorophylls in Monolayers. Infrared Study of Chlorophyll a in a Mono- and Multilayer Arrays. chem. phys. lett. 49: 180-182.
[31] Leblanc RM, Chapados C (1977) Aggregation of Chlorophylls in Monolayers. biophys. chem. 6: 77-85.
[32] Chapados C, German D, Leblanc RM (1980) Aggregation of Chlorophylls in Monolayers: IV. The Reorganization of Chlorophyll a in Multilayer Array. biophys. chem. 12: 189-198.

[33] Jagadeesh Babu Veluru SK (2007) Electrical Properties of Electrospun Fibers of PANI-PMMA Composites. journal of engineered fibers and fabrics 2(2): 25-31.
[34] Project Ingenhousz: Light, Genes and Molecular Machines. Retrieved from http://dwb.unl.edu/Teacher/NSF/C11/C11Links/photoscience.la.asu.edu (Accessed 30/04/99)
[35] Mapel JK (2006) The Application of Photosynthetic Materials and Architectures to Solar Cells. California: Massachusetts Institute of Technology.
[36] Boussaad S, Tazi A, Leblanc RM (1999) Study of the Conformational Changes of Chlorophyll a (Chl a) Colloids with the Atomic Force Microscope. j. of colloid and interface science 209: 341-346.
[37] Cullity B (1956) Elements of X-Ray Diffraction. USA: Addison-Wesley Publishing Company Inc.
[38] Dharmadhikari CV, Ali AO, Suresh N, Phase DM, Chaudhari SM, Gupta A, Dasannacharya BA (2000) A Comparison of Nucleation and Growth Investigations of Thin Films using Scanning Tunneling Microscopy, Atomic Force Microscopy and X-ray Scattering. materials science and engineering b 75(1): 29-37.